Journal of Solid State Chemistry **147,** 536–544 (1999)
Article ID jssc.1999.8414, available online at http://www.idealibrary.com on IDEAL®

Intergrowth Tungsten Bronze Structures of Pr_xWO_3, Formed at 50 kbar: An HRTEM Study

N. D. Zakharov,* P. Werner,* I. P. Zibrov,† V. P. Filonenko,‡ and M. Sundberg§

*Max Planck Institute for Microstructure Physics, Weinberg 2, D-06120 Halle/Saale, Germany; †Institute of Crystallography, Russian Academy of Sciences, 117333 Moscow, Russia; ‡Institute for High Pressure Physics, Russian Academy of Sciences, Troitsk, 142092 Moscow Region, Russia; and §Department of Inorganic Chemistry, Arrhenius Laboratory, Stockholm University, S-10691 Stockholm, Sweden

Received February 11, 1999; in revised form May 28, 1999; accepted June 8, 1999

New praseodymium intergrowth tungsten bronzes, Pr_xWO_3, of (n)-ITB structure type have been prepared by solid state reaction at $P = 50$ kbar and $T = 1570$ K. The ordered members $n = 2$, 3, and 4 were identified by high-resolution transmission electron microscopy. The structure of (2)-ITB was deduced from an electron micrograph, and the unit cell parameters were determined from the X-ray powder data: $a = 10.17$ Å, $b = 7.418$ Å, and $c = 3.790$ Å. The praseodymium content ($0.04 \leq x \leq 0.1$), corresponding to less than half-filled hexagonal tunnels in the ITB-structures, was found by combining electron diffraction and microanalysis studies of the same crystal fragments. An ordered superstructure, designated $(2)_5(3)_3$-ITB, was also observed.

INTRODUCTION

The possibility of preparing several new binary tungsten oxides by solid state reaction under high pressure and high temperature conditions has been demonstrated in our previous publications (1–4). These studies showed that the application of high pressure ($P = 50$–80 kbar) during the preparation process considerably changes the phase equilibrium in the tungsten–oxygen system and results in the formation of the new phases W_3O_8(I), W_3O_8(II), $WO_{2.625}$, $\sim WO_{2.5}$, and hp-WO_2. By similar experiments in the Nd_2O_3–WO_3 system ($P = 50$ kbar and $T = 1520$ K), we have synthesized compounds with intergrowth tungsten bronze (ITB) and hexagonal tungsten bronze (HTB) type structures (5). It has not been possible to prepare such phases by solid state reaction at high temperature and ambient pressure. The latter experimental conditions result in the formation of some perovskite tungsten bronzes, RE_xWO_3 (RE = Ce–Lu and $x \approx 0.1$) (6–8).

The crystal structure of the hexagonal tungsten bronze, A_xWO_3, is built up from WO_6 octahedra joined by corners, forming hexagonal tunnels in which the A atoms are located (9). It has been found previously that the HTB-structure is formed with the larger alkali metals (A = K, Rb, and Cs and $x = 0.19$–0.33) and with monovalent cations of thallium and indium (10, 11). Hexagonal tungsten bronzes of the alkaline earths metals Ca, Sr, and Ba have also been prepared under high pressure (12, 13).

The HTB structure becomes unstable at lower alkali concentrations ($x < 0.10$), and the intergrowth tungsten bronze (ITB) structure is formed instead. This structure type consists of alternating HTB and WO_3 slabs (10, 14). The slabs of WO_3-type can have different widths (n) and are intergrown with single or double slices of the HTB structure. According to the nomenclature introduced by Hussain and Kihlborg (14), single hexagonal tunnel row structures are denoted (n)-ITB, while ITB-phases containing double tunnel rows are designated ($1, n$). Considerable disorder due to variation in width of the two structural constituents has been seen in HREM images (15). A large variation of tunnel occupancy in the intergrowth tungsten bronzes, A_xWO_3 (A = Cs, Sn, Sb) has also been observed by some authors (16–18). Both ordered and defect structures of (2)-ITB were recently found for the neodymium tungsten bronzes, $(Nd,Ca)_xWO_3$, prepared at 50 kbar (5).

The present work is an investigation of the phase composition and the phase structures in a praseodymium-containing tungsten-bronze sample synthesized by solid-state reaction under high-pressure conditions by high-resolution transmission electron microscopy (HRTEM).

EXPERIMENTAL

The sample was prepared by heating a pellet of a finely ground mixture of 90 wt% WO_3 and 10 wt% Pr_2O_3 in a graphite container in a high-pressure apparatus at $P = 50$ kbar, $T = 1570$ K. A detailed description of the experimental setup is given in Ref. (19). The graphite caused a very low oxygen pressure, thus reducing conditions at the sample. The X-ray powder diffraction pattern was taken with a Guinier–Hägg camera using Cu$K\alpha$ radiation and silicon as internal standard.

0022-4596/99 $30.00

The electron microscopy specimens were prepared by crushing a small amount of the sample in an agate mortar, dispersing the resulting fine powder in acetone, and putting drops of the suspension on a holey carbon film supported on a Cu grid. The phase composition and structure type were investigated by electron diffraction combined with energy-dispersive X-ray spectroscopy (EDX) on the individual crystal fragments. Electron microscopes, Philips CM20T with EDX (Voyager I, Ge detector) and JEOL 2000FXII with Link OX-200 (Si detector), were used for the microanalysis studies. The results are based on the W*L* and Pr*L* lines in the EDX-spectra. As concerns the precision in the EDX-analyses, repeated measurements on the same crystal fragment gave a variation within $\pm 5\%$. The crystal structure was obtained from high-resolution transmission electron microscopy (HRTEM) images taken in a JEOL JEM-4000 EX microscope. The DigitalMicrograph 2.0 software was used for image filtration and processing. Theoretical images of the structure models were simulated with the MacTempas program (20). The structure models were drawn with ATOMS by Shape Software.

RESULTS

Both the X-ray powder pattern and the HRTEM study showed a multiphase sample. Three members, $n = 2$, 3, and 4, of the (n)-ITB family of related phases were identified from their electron diffraction patterns. The first member, (2)-ITB, was more often observed, and its unit cell parameters could be calculated from the X-ray powder data: $a = 10.17$ Å, $b = 7.418$ Å, and $c = 3.790$ Å. It should be noted that some unindexed lines in the X-ray powder pattern could be assigned to an HTB-phase with the unit cell dimensions $a = 7.398$ Å and $c = 7.583$ Å, but such crystals have not yet been seen by HRTEM.

a. (2)-ITB

An HRTEM image, the corresponding electron diffraction pattern, and the structure model of the (2)-ITB phase in [001] projection are shown in Figs. 1a and 1b. The image was taken close to Scherzer conditions where the dark spots correspond to cation positions. The micrograph clearly illustrates that the WO_3 slabs are two octahedra wide ($n = 2$), because slabs consisting of two rows of dark spots are regularly seen in the image. Figure 1a also shows a variation of the filling of the hexagonal tunnels (see, for example, tunnels at E and F). The white contrast (E) indicates empty tunnels, and the dark dots at F probably indicate completely filled ones. Furthermore, partially filled tunnels seem to be arranged in (010) planes, resulting in the appearance of horizontal streaks (marked S) in the picture. A close inspection of the HRTEM image shows that some of the dark dots are slightly displaced from the center of the six-sided tunnels, which suggests that the Pr atoms can occupy an off-center tunnel position. In order to reveal the atom positions more accurately the experimental image was filtered by a Fast Fourier Transform (FFT) procedure. This corresponds to averaging the contrast over about 200 unit cells. The tungsten and oxygen atom positions were deduced from the processed image in Fig. 1c. There is a good accordance between experimental and theoretical images, as can be seen in Fig. 1d, for the set of coordinates listed in Table 1. The correctness of the structure model of (2)-ITB shown in Fig. 1b was checked by calculation of the interatomic W–W, W–O, and O–O distances. The praseodymium atoms are located in the center of the six-sided tunnels of the model in Fig. 1b. It should be noted that the EDX results give less than half-filled tunnels.

Unfortunately, we failed to get an electron diffraction pattern of (2)-ITB in the [010] orientation, but we succeeded in aligning a crystal along [012], as can be seen in Fig. 2a. This orientation is obtained by rotating the unit cell 45° around the a-axis from [001]. The appearance of weak odd reflections in the diffraction pattern indicates that the cell in this projection is centered, with a size of 20.3 and 5.3 Å. These values correspond to a unit cell with doubled a- and c-axes ($a = 2 \times 10.17 = 20.34$ Å and $c = 2 \times 3.79 = 7.58$ Å). Weak superstructure spots which indicate a doubling of the c-axis have previously been seen in electron diffraction patterns taken in the [010] orientation of alkali ITB-crystals (14).

In the thinner region of the HRTEM image (Fig. 2a) it is possible to observe an ordered arrangement of pairs of dark dots closer together in the planes corresponding to the hexagonal tunnel rows in the structure (see arrows). The observed contrast features indicate an ordered displacement of the praseodymium atoms from the tunnel center. In the plausible structure model in Figs. 2b and 2c, the Pr atoms have been shifted approximately 0.3 Å along the b-axis and 0.1 Å along the c-axis. Figure 2c shows pairs of atoms closer together along the hexagonal tunnel rows in the structure projected along $[012]_{\text{subcell}}$. A simulated image of the suggested structure model is also in good agreement with the observation made in the HRTEM image.

Furthermore, about half of the recorded electron diffraction patterns along [001] of the (2)-ITB crystals showed weak odd reflections (Fig. 3), which indicate a doubling of the unit cell parameters $a = 2 \times 10.14 = 20.28$ Å and $b = 2 \times 7.4 = 14.8$ Å. It was impossible to take HRTEM images of these crystals, because the short-range order in the structure was unstable and disappeared under the high intensity of the electron beam used to get the image.

When all hexagonal tunnel positions are occupied by praseodymium, the stoichiometric composition of the (2)-ITB structure (Fig. 1b) is PrW_5O_{15}. This means that x in the formula Pr_xWO_3 cannot exceed 0.2. In order to determine the value of x and thus the occupancy of the tunnel

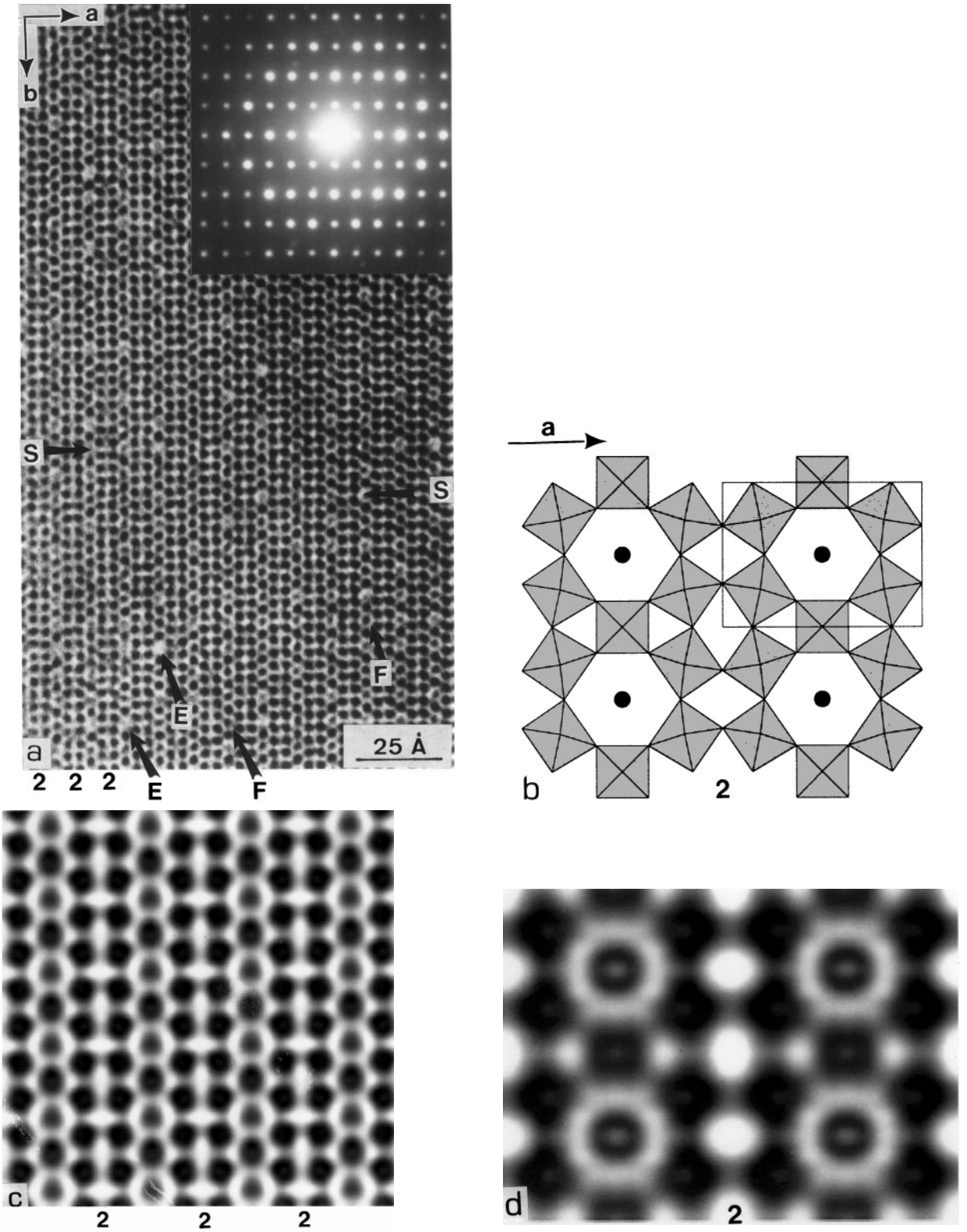

FIG. 1. (a) HRTEM image of $Pr_{\sim 0.08}WO_3$, showing an ordered (2)-ITB phase in [001] projection. The corresponding electron diffraction pattern is inserted. E and F represent hexagonal tunnels which are likely to be empty and completely filled. White streaks (S) parallel to [100] are due to rows of partially filled tunnels. (b) Structure model of (2)-ITB deduced from the HRTEM image in (a). The black spots in the middle of the tunnels represent praseodymium atoms. (c) Fourier-filtered image of a region (approximately 200 unit cells) in (a). (d) Theoretical HRTEM image calculated from the structure model in (b). Crystal thickness, 24 Å; defocus value, −450 Å.

TABLE 1

Approximate Atomic Coordinates for Pr_xWO_3 ((2)-ITB structure), Obtained from the Processed HRTEM image (a = 10.17 Å, b = 7.418 Å, and c = 3.79 Å, space group $P222$)

Atom	x/a	y/b	z/c
Pr 1	1/2	1/2	1/2
W 1	1/2	0	0
W 2	0.19	0.26	0
O 1	0.15	0	0
O 2	0	0.30	0
O 3	0.37	0.18	0
O 4	0.21	1/2	0
O 5	1/2	0	1/2
O 6	0.19	0.26	1/2

positions, electron diffraction patterns and EDX-analyses were taken from the same crystal fragments. Of special interest was to relate the appearance of weak superstructure reflections in the diffraction patterns with the composition of the crystal. The EDX-results showed that the (2)-ITB phase is formed for $0.04 \leq x \leq 0.1$, and it follows that less than half of the available atom positions are occupied by praseodymium. It should be noted that no impurity peaks were observed in the EDX spectra. Weak superstructure reflections (see above) were observed in the electron diffraction patterns taken from approximately half of the investigated crystals, but no clear correlation between the appearance of superstructure reflections and the composition was observed.

In order to investigate the local ordering of praseodymium in the tunnels, we measured the intensity variation of the black spots along an hexagonal tunnel row in the experimental image as indicated in Fig. 4a. The intensities were measured in the scanned image by averaging over a 1×1 Å square region centered on the corresponding cation position. One can clearly see in Fig. 4b that the intensities of the W positions do not vary very much, whereas the intensities of the Pr atom positions in the hexagonal tunnels change drastically. This fact indicates different occupancy of the hexagonal tunnel sites by praseodymium. Figure 4b also shows that the occupancy varies more or less periodically, and usually highly occupied tunnels (lower intensity) alternate with those of lower occupancy (high intensity). An ordered arrangement of Pr atoms and vacancies in the tunnels will give rise to weak superstructure spots in the electron diffraction patterns like those seen in Fig. 3.

b. (3)-ITB

Some crystal fragments showing an ordered (3)-ITB phase were also observed in the Pr_xWO_3 sample. The HRTEM image, the corresponding electron diffraction pattern, and the structure model are illustrated in Figs. 5a–5c, respectively. According to the diffraction pattern (Fig. 5b) the unit cell is C-centered and has the unit cell parameters $a \approx 27.5$ Å and $b \approx 7.4$ Å. The structure (Fig. 5c) contains rows of hexagonal tunnels which are separated by WO_3 slabs, three octahedra wide. The stoichiometric composition is PrW_7O_{21} ($Pr_{0.14}WO_3$) when all hexagonal tunnel positions are fully occupied by praseodymium. EDX analyses of (3)-ITB fragments showed approximately half-filled tunnels. It should be pointed out that we did not observe a strong contrast variation of the hexagonal tunnel spots in the HRTEM images, as in the (2)-ITB structure. This suggests that the tunnels are almost uniformly occupied by praseodymium in the (3)-ITB structure.

c. (4)-ITB

The electron diffraction pattern in Fig. 6a shows a well-ordered (4)-ITB phase. Such patterns were taken from a few crystal fragments. The unit cell dimensions of (4)-ITB were found to be $a \approx 17.8$ Å, $b \approx 7.4$ Å, and $c \approx 3.8$ Å, and also in this case the EDX-analyses showed approximately half-filled hexagonal tunnels. The HRTEM image in Fig. 6a, taken close to Scherzer conditions of a somewhat thicker crystal than that in Fig. 1a, shows a well-ordered crystal with all hexagonal tunnels partly occupied. The black spots corresponding to the projected metal atoms have almost the same darkness, which indicates that praseodymium atoms (ions) and vacancies are fairly evenly distributed over the hexagonal tunnels. The WO_3 slabs are four octahedra wide in the (4)-ITB structure (Fig. 6b), and the stoichiometric composition corresponds to PrW_9O_{27} ($Pr_{0.11}WO_3$). The EDX-results of examined fragments indicate a composition of $\sim Pr_{0.05}WO_3$.

d. Intergrowth Structures

Most of the examined crystals seemed to be free from large structural defects such as WO_3-type slabs of different widths and wider HTB-type slabs. However, we have found one crystal showing a structure with long-range order (Fig. 7). The substructure reflections in the electron diffraction pattern correspond to the (2)-ITB structure. The sharpness of the superstructure spots indicates that the superstructure extends over a large region. Unfortunately the crystal was too thick to give an atomic-resolution image, but even so, it is possible to distinguish an ordered intergrowth of five slabs of the (2)-ITB phase with three slabs of the (3)-ITB structure. This superstructure will be designated $(2)_5(3)_3$-ITB according to the notation introduced by Hussain and Kihlborg (14). The unit cell dimensions of $(2)_5(3)_3$-ITB are $a \approx 185$ Å, $b \approx 7.4$ Å, and $c \approx 3.8$ Å (projection axis).

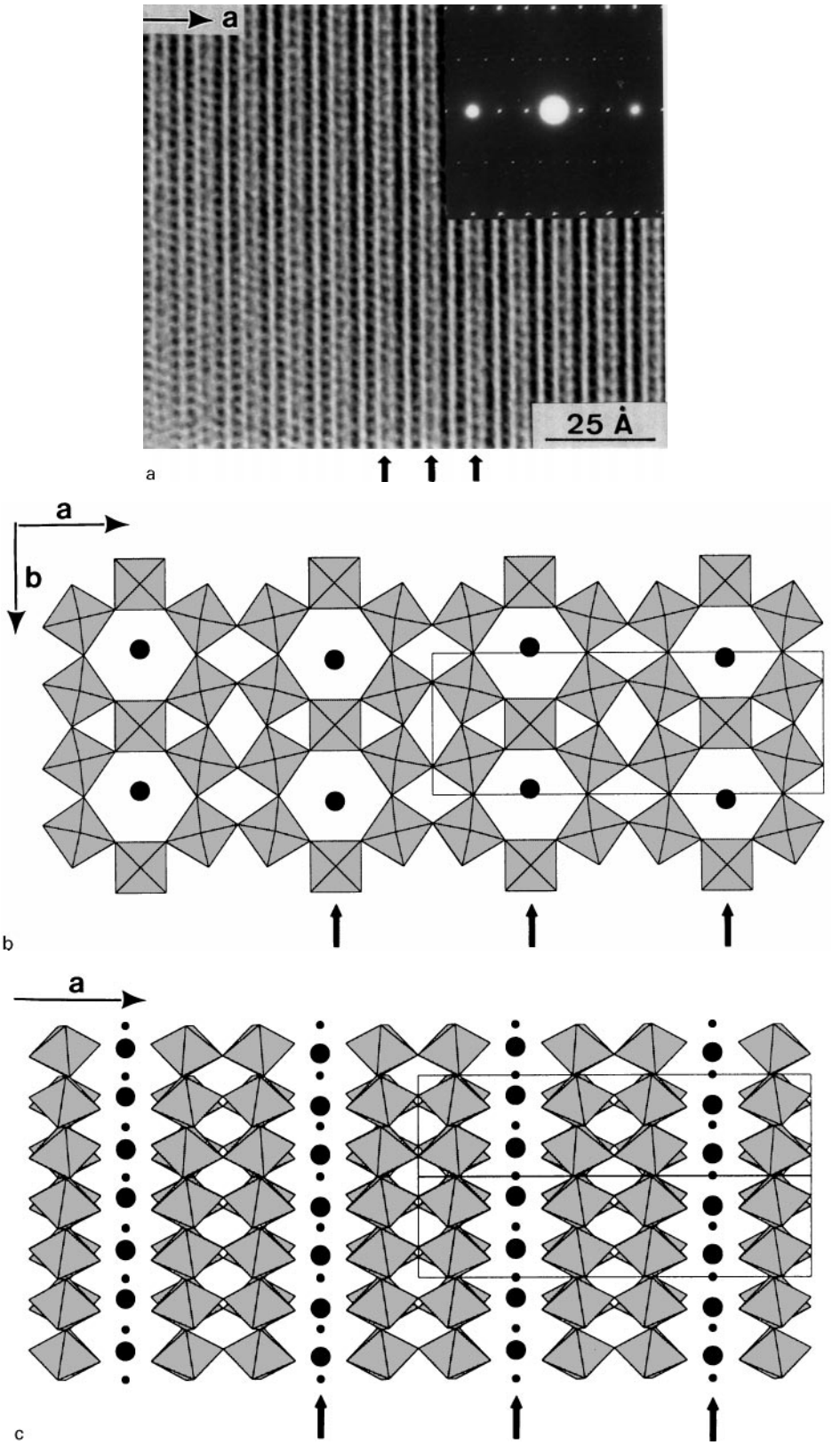

FIG. 2. (a) HRTEM image of a Pr_xWO_3 crystal projected along [012]. The corresponding electron diffraction pattern is inserted. A plausible structure model of (2)-ITB with the Pr atoms displaced from the tunnel center, projected along (b) [001] and (c) [012] ($c \approx 3.8$ Å). The hexagonal tunnel rows are marked by arrows. The large black spots represent Pr atoms, and the small black dots show W atoms.

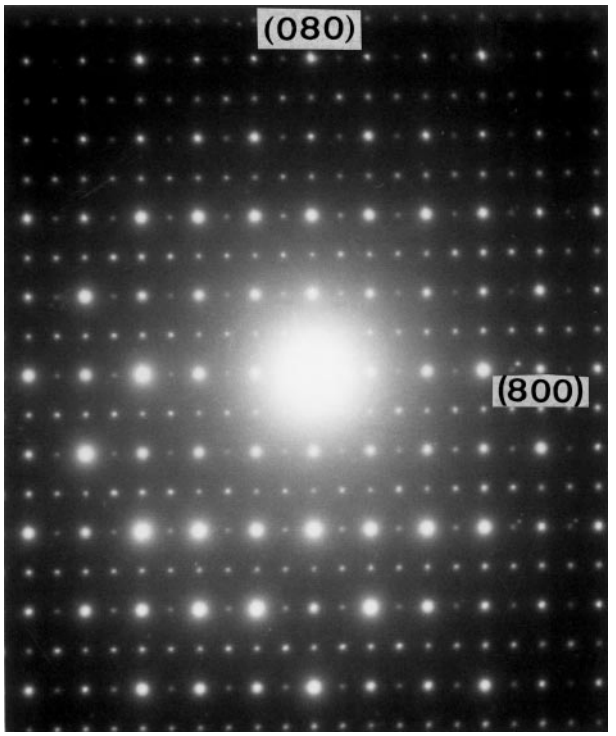

FIG. 3. The electron diffraction pattern of a 2-ITB crystal shows weak superstructure spots, which indicate a doubling of the *a*- and *b*-axes parameters.

DISCUSSION

This study has shown that praseodymium intergrowth tungsten bronzes, Pr_xWO_3, prepared under high-pressure and high-temperature conditions form ordered members of the (*n*)-ITB family of related phases with $n = 2$, 3, and 4. The HRTEM images indicate that the Pr atoms (ions) in the six-sided tunnels might be locally shifted from the tunnel center in the $\pm[010]$ and $\pm[001]$ directions. Similar shifts of indium atoms (ions) have been observed by Labbé *et al.* in the hexagonal tungsten bronzes of indium (11). In the latter compounds, the In^{1+} cations occupy one of six off-center positions in the tunnels, which are actually sixfold degenerated due to crystal symmetry. However, this was considered to be related to the presence of the lone pair of In^{1+}.

In the praseodymium ITB-bronzes the hexagonal tunnels seem to be slightly elongated in the [010] direction. This probably means that there will be two off-axis positions that correspond to sites of minimum energy. A displacement of the praseodymium atom from the tunnel center can be explained by the small ionic radius of Pr^{3+} ($r \approx 1.29$ Å (21)), which is even less than that of In^{1+} ($r = 1.35$ Å (11)) and much less than the radius of the cavity. It is interesting to note that Jefferson *et al.* (22) have observed a slight displacement of the Bi atoms within the hexagonal tunnel in an HREM image of an (8)-ITB crystal from a $Bi_{0.1}WO_3$ sample. Isotypic tungsten bronzes, A_xWO_3, of (*n*)-ITB structure type have also been reported for $A =$ Cs, Ba, Sn, and Pb (15, 23).

There is a strong similarity between the ordered Pr_xWO_3 bronzes of (*n*)-ITB structure type with $n = 2$, 3, and 4 and

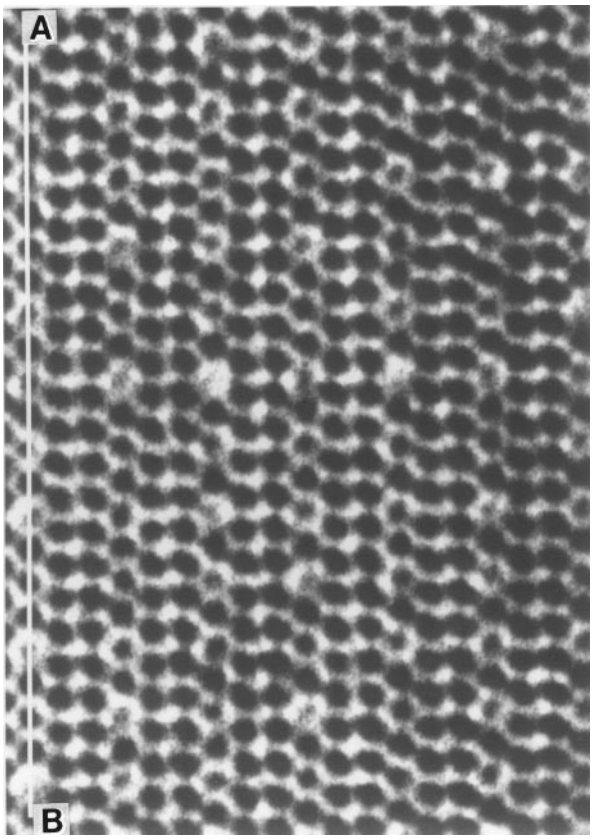

FIG. 4. (a) HRTEM image of (2)-ITB taken close to Scherzer defocus. (b) Variation of the intensities on a logarithmic scale at Pr (dotted) and W (black) positions measured along AB in (a).

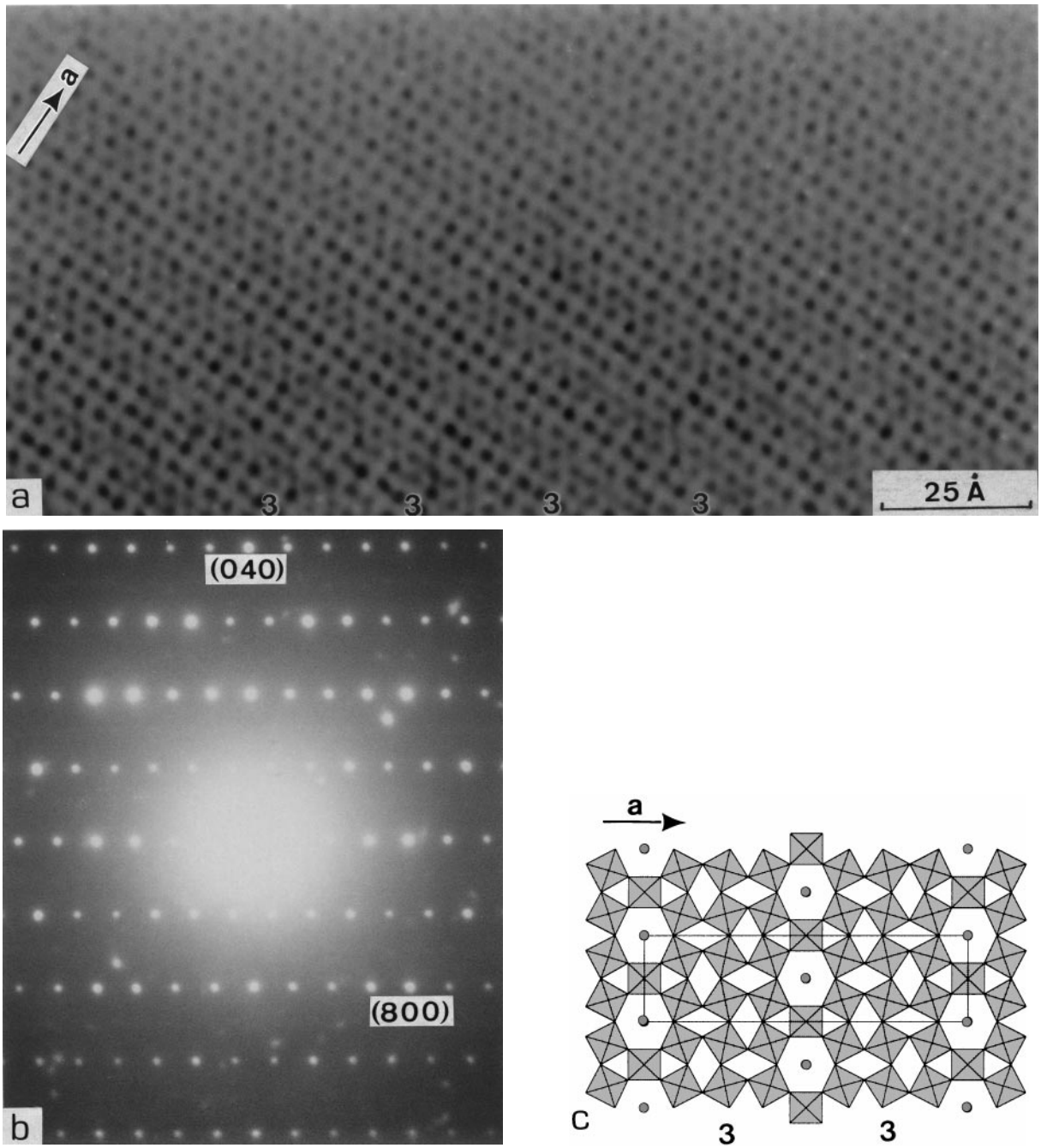

FIG. 5. (a) HRTEM image of a Pr_xWO_3 crystal with $x \approx 0.06$. (b) The corresponding electron diffraction pattern shows a (3)-ITB structure projected along the *c*-axis ($c \approx 3.8$ Å). (c) The crystal structure of (3)-ITB. The black spots represent the Pr atoms.

the complex uranium–molybdenum and uranium–molybdenum–tungsten oxides of (*n*)-HB structure type with $n = 2$, 3, and 4 (23, 24). The structures have the same basic framework and differ only in the filling of the hexagonal tunnels. In the praseodymium bronzes there are both ordered and disordered arrangements of praseodymium atoms and vacancies in the tunnels, whereas in the uranium compounds the six-sided tunnels are filled by –U–O–U–O– atom strings in such a way that hexagonal UO_8-bipyramids (HB:s) are formed. Different ordered arrangements of uranium atoms and vacancies in the six-sided tunnels give rise to different types of superstructures, which seem to be similar to those observed for the Pr_xWO_3 bronzes.

There is an obvious difference between the results obtained in this study on the Pr_xWO_3 bronzes and those previously reported on the ITB bronzes containing

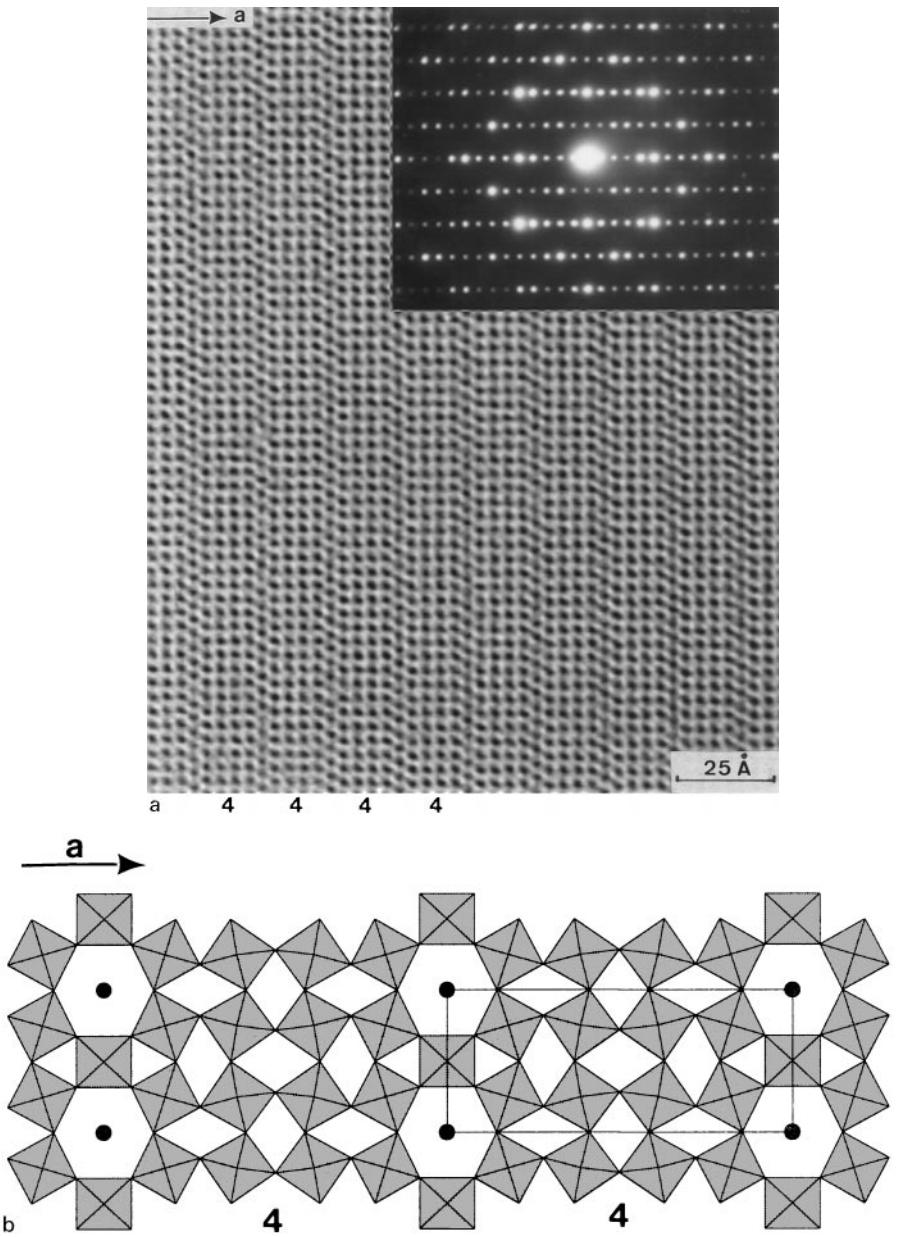

FIG. 6. (a) HRTEM image of a $Pr_{\sim 0.05}WO_3$ crystal projected along the *c*-axis. The corresponding electron diffraction pattern is inserted. (b) The crystal structure of (4)-ITB with the praseodymium atoms shown as dark spots.

neodymium (5), despite the fact that the samples were prepared under the same conditions. The Pr_xWO_3 bronzes formed well-ordered (*n*)-ITB phases with $n = 2$, 3, and 4, whereas both ordered and defect-rich structures of (2)-ITB type were observed in the Nd-containing crystals. The latter crystals contained, however, a small amount of calcium due to the reaction of the sample with the high-pressure chamber wall during the synthesis. The difference in structures might therefore be due to the presence of calcium in the neodymium case. Calcium has previously been observed to contribute to formation of an HTB bronze structure under high-pressure conditions (12, 13). The ionic radii of Pr^{3+} ($r \approx 1.29$ Å), Nd^{3+} ($r \approx 1.27$ Å), and Ca^{2+} ($r \approx 1.34$ Å) (21) are similar, but the valence state of calcium differs from those of the other two elements. Thus the $(Nd,Ca)_xWO_3$ crystals contain tunnel ions of mixed oxidation states, which might be important for the formation of the defect structures. The results warrant further investigations, under carefully controlled high-pressure and high-temperature conditions, of the formation of Nd_xWO_3, Ca_xWO_3, and $(Pr,Ca)_xWO_3$ bronzes. Such experiments are now underway.

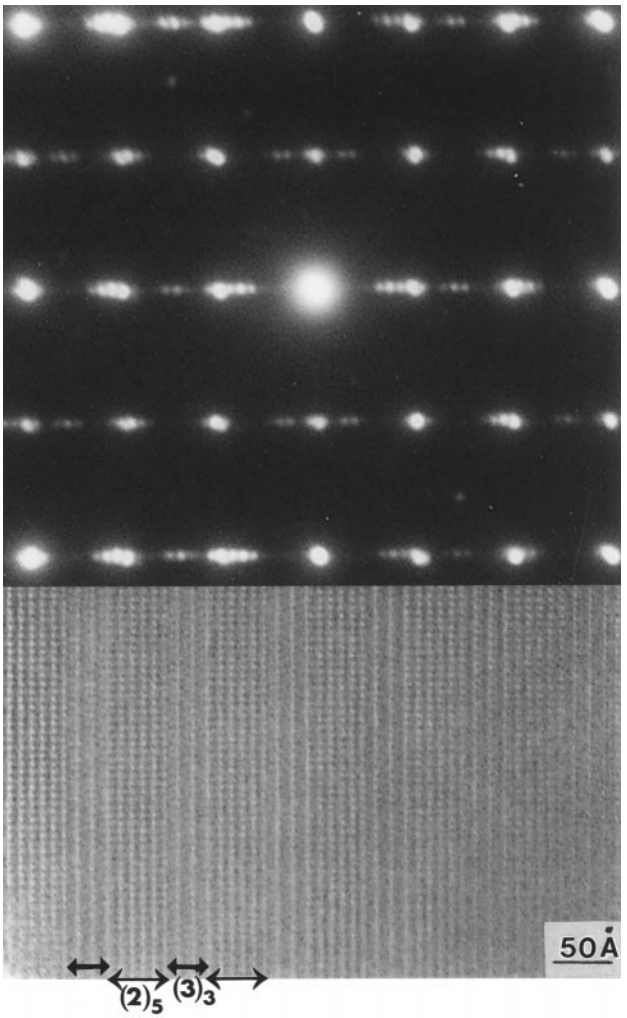

FIG. 7. The HRTEM image of a fairly thick Pr_xWO_3 crystal shows an ordered superstructure of (*n*)-ITB type. The corresponding electron diffraction pattern is inserted ([001] zone).

ACKNOWLEDGMENTS

We wish to thank Professor L. Kihlborg for stimulating discussions and valuable comments on the manuscript. This study has partly been performed within a program for Swedish-Russian joint research projects. Financial support from the Royal Swedish Academy of Sciences and from the Swedish Natural Science Research Council is gratefully acknowledged.

REFERENCES

1. M. Sundberg, N. D. Zakharov, I. P. Zibrov, Yu. A. Barabanenkov, V. P. Filonenko, and P. Werner, *Acta Crystallogr. Sect. B* **49,** 951 (1993).
2. Yu. A. Barabanenkov, N. D. Zakharov, I. P. Zibrov, V. P. Filonenko, P. Werner, A. I. Popov, and M. D. Valkovskii, *Acta Crystallogr. Sect. B* **49,** 169 (1993).
3. V. P. Filonenko, I. P. Zibrov, and M. Sundberg, "High Pressure Science and Technology, Proceedings, Joint XV AIRAPT and XXXIII EHPRG International Conference," 110, 1996.
4. M. Sundberg, P.-E. Werner, and I. P. Zibrov, *Z. Kristallogr.* **209,** 662 (1994).
5. N. D. Zakharov, Z. Liliental-Weber, V. P. Filonenko, I. P. Zibrov, and M. Sundberg, *Mater. Res. Bull.* **31,** 373 (1996).
6. W. Ostertag, *Inorg. Chem.* **5,** 758 (1966).
7. C. S. Dimbylow, I. J. McColm, C. M. P. Barton, N. N. Greenwood, and G. E. Turner, *J. Solid State Chem.* **10,** 128 (1974).
8. I. N. Belyaev, and L. A. Voropanova, *Zh. Neorg. Khim.* 3107 (1976).
9. A. Magnéli, *Acta Chem. Scand.* **7,** 315 (1953).
10. A. Hussain, *Acta Chem. Scand.* **A32,** 479 (1978).
11. Ph. Labbé, M. Goreaud, B. Raveau, and J. C. Monier, *Acta Crystallogr. Sect. B* **34,** 1433 (1978).
12. P. E. Bierstedt, T. A. Bither, and F. J. Darnell, *Solid State Commun.* **4,** 25 (1966).
13. T. A. Bither, J. L. Gillson, and H. S. Young, *Inorg. Chem.* **5,** 1559 (1966).
14. A. Hussain and L. Kihlborg, *Acta Crystallogr. Sect. A* **32,** 551 (1976).
15. L. Kihlborg, *Chem. Scr.* **14,** 187 (1978–1979).
16. A. Hussain, *Chem. Scr.* **11,** 224 (1977).
17. T. Ekström and R. J. D. Tilley, *J. Solid State Chem.* **24,** 209 (1978).
18. T. Ekström, M. Parmentier, and R. J. D. Tilley, *J. Solid State Chem.* **34,** 397 (1980).
19. I. P. Zibrov, V. P. Filonenko, P.-E. Werner, B.-O. Marinder, and M. Sundberg, *J. Solid State Chem.* **141,** 205 (1998).
20. R. Kilaas, "Proceedings, 45th Annual EMSA Meeting, San Francisco," p. 66, 1987.
21. R. D. Shannon, *Acta Crystallogr.* **A32,** 751 (1976).
22. D. A. Jefferson, M. K. Uppal, D. J. Smith, J. Gopalakrishnan, A. Ramanan, and C. N. R. Rao, *Mater. Res. Bull.* **19,** 535 (1984).
23. M. M. Dobson, J. L. Hutchison, R. J. D. Tilley, and K. A. Watts, *J. Solid State Chem.* **71,** 47 (1987).
24. V. V. Tabachenko, O. G. D'yachenko, and M. Sundberg, *Eur. J. Solid State Inorg. Chem.* **32,** 1137 (1995).
25. M. Sundberg and V. V. Tabachenko, *Microsc. Microanal. Microstruct.* **1,** 373 (1990).